High-T_c DC SQUIDs for Magnetoencephalography

M. I. Faley, U. Poppe, R. E. Dunin-Borkowski, M. Schiek, F. Boers, H. Chocholacs, J. Dammers, E. Eich, N. J. Shah, A. B. Ermakov, V. Y. Slobodchikov, Y. V. Maslennikov, and V. P. Koshelets

***Abstract*—We have investigated the microstructural and electron transport properties of 45° step-edge Josephson junctions grown on MgO substrates and used them for the preparation of superconducting quantum interference device (SQUID) magnetometers intended for magnetoencephalography (MEG) measurement systems. The high-T_c SQUID magnetometers also incorporate 16 mm multilayer superconducting flux transformers on the MgO substrates and demonstrate a magnetic field resolution of $\sim$4 fT/$\sqrt{\text{Hz}}$ at 77 K. Results are illustrated for the detection of auditory evoked magnetic responses of the human cortex and compared between high-T_c SQUIDs and a commercial low-T_c MEG system. Our results demonstrate that MEG systems can be upgraded using high-T_c SQUIDs to make them independent of helium and more user-friendly, saving operating costs and leading to the widespread utilization of MEG systems in clinical practice and at universities.**

***Index Terms*—Josephson junctions, magnetoencephalography (MEG), magnetometers, superconducting quantum interference devices (SQUIDs).**

I. Introduction

MAGNETOENCEPHALOGRAPHY (MEG) systems are currently based on low-T_c superconducting quantum interference devices (SQUIDs), which are cooled by liquid helium. Helium prices have risen by ≈300 per cent recently and are expected to grow further [1]–[4]. The increasing cost of liquid helium is one of the main obstacles for the acceptance of MEG in research and clinical practice. Typically, the magnetic field resolution of low-T_c MEG systems is $\sim$4 fT/$\sqrt{\text{Hz}}$ at 4.2 K and is determined by the Nyquist noise of the cryostat and the magnetically shielded room (MSR) [5], [6]. For most routinely used MEG systems, a magnetic field resolution of better than 10 fT/$\sqrt{\text{Hz}}$ in the frequency range 1 Hz to 1 kHz would be sufficient. Multilayer high-T_c SQUIDs are able to fulfill these requirements.

High-T_c SQUIDs do not need helium for cooling. However, making them sufficiently sensitive for MEG is challenging. Single-layer direct-coupled high-T_c SQUIDs with an intrinsic white noise exceeding 10 fT/$\sqrt{\text{Hz}}$ at 77 K have previously been tested for the recording of MEG signals [7]–[9]. The time required to obtain sufficiently high signal-to-noise ratio for MEG measurements with such sensors, for a practical SQUID-to-scalp separation of about 15 mm and magnetic fields emanating from deeper sources, would be too long. Smaller separations, such as that described in [9], are problematic to realize in helmet-type cryostats for whole-head multichannel systems.

Much better magnetic field resolution can be achieved by using a multiturn input coil, due to the improved transformation of the measured magnetic field into magnetic flux penetrating through the SQUID loop. For a SQUID inductance $\sim$160 pH and a 16 mm pick-up coil, the effective area A_{eff} of such magnetometers exceeds the effective area A_{eff} of a direct-coupled DC SQUID magnetometer with a similar size of pick-up coil by about 7 times. High-T_c SQUIDs with multilayer flux transformers have a good chance of being used as magnetic field sensors in future MEG systems because they have a magnetic field resolution of $\sim$4 fT/$\sqrt{\text{Hz}}$ at 77 K for a 16 mm sensor [10]–[12], the ability to measure vector components and spatial gradients of magnetic fields, the ability to resolve small changes in large signals, and a white noise spectrum across a wide frequency range. The use of readily available and relatively cheap step-edge Josephson junctions on single crystal substrates instead of bicrystal Josephson junctions can further improve the sensitivity and reduce the cost of high-T_c sensors. However, better control of the parameters of the junctions is required. Here we describe the microstructural and electron transport properties of multilayer high-T_c DC SQUID magnetometers with step-edge Josephson junctions and compare MEG measurements obtained using a high-T_c system with those obtained using a commercial low-T_c system.

II. Experimental Details

The high-T_c DC SQUID flip-chip magnetometers used in our experiments were fabricated by high-oxygen-pressure magnetron sputtering [11], [13] from stoichiometric polycrystalline targets. An image of the inner part of a SQUID structure, taken using a scanning electron microscope (SEM), is shown in Fig. 1. The DC SQUIDs were made from 150-nm-thick films of $YBa_2Cu_3O_{7-x}$ (YBCO) and consisted of two $\sim$1.5-μm-wide step-edge Josephson junctions, one 1 mm washer and one 3 mm direct-coupled pickup loop integrated on a 10 mm × 10 mm × 1 mm MgO (001) substrate. Step-edge junctions on 300 nm high substrate steps were prepared by using masks of AZ TX1311 photoresist patterned by deep-UV lithography, using a two-part milling process [14] with Ar ion beam etching (IBE) at 100 V. A 16 mm multilayer

Manuscript received October 8, 2012; accepted October 30, 2012. Date of publication November 20, 2012; date of current version January 5, 2013.

M. I. Faley, U. Poppe, R. E. Dunin-Borkowski, M. Schiek, F. Boers, H. Chocholacs, J. Dammers, E. Eich, and N. J. Shah are with Forschungszentrum Jülich GmbH, D-52428 Jülich, Germany (e-mail: m.faley@fz-juelich.de; U.Poppe@fz-juelich.de; r.dunin-borkowski@fz-juelich.de; m.schiek@fz-juelich.de; f.boers@fz-juelich.de; h.chocholacs@fz-juelich.de; j.dammers@fz-juelich.de; e.eich@fz-juelich.de; n.j.shah@fz-juelich.de).

A. B. Ermakov, V. Y. Slobodchikov, Y. V. Maslennikov, and V. P. Koshelets are with The Kotel'nikov Institute of Radio Engineering and Electronics RAS, 125009 Moscow, Russian Federation (e-mail: ermakov@hitech.cplire.ru; slb@inbox.ru; cryoton@inbox.ru; valery@hitech.cplire.ru).

Color versions of one or more of the figures in this paper are available online at http://ieeexplore.ieee.org.

Digital Object Identifier 10.1109/TASC.2012.2229094

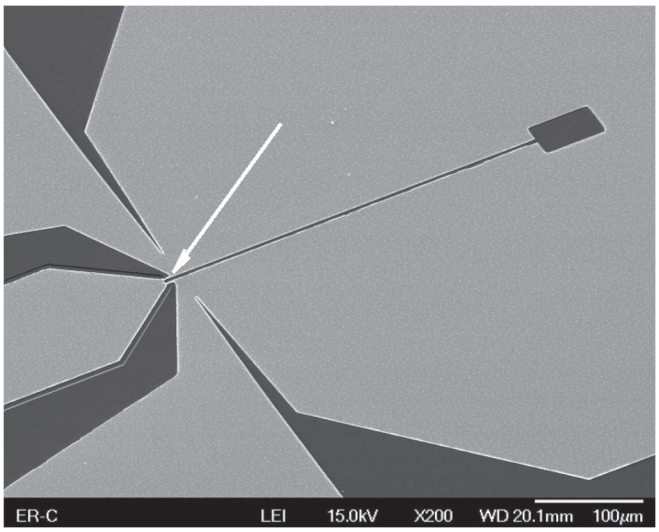

Fig. 1. SEM image of a dc SQUID with two step-edge Josephson junctions, a 1-mm washer and a 3-mm direct-coupled pickup loop. The position of the step-edge junctions is marked by an arrow.

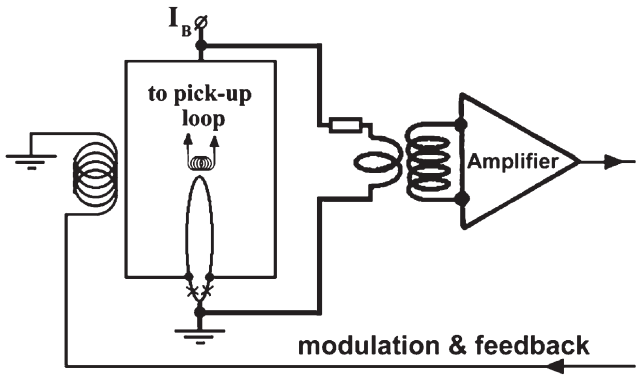

Fig. 2. Schematic diagram of the SQUID flip-chip magnetometer with coupling to control electronics.

superconducting flux transformer was prepared using YBCO, $PrBa_2Cu_3O_{7-x}$ (PrBCO) and $SrTiO_3$ (STO) films on a single crystal round MgO (001) wafer of diameter 30 mm and thickness 1 mm buffered by epitaxial $BaZrO_3$ and STO films [15] and assembled together with the SQUID in a flip-chip configuration [16].

For assembling the DC SQUID flip-chip magnetometers, the SQUID washer was inductively coupled to the 14-turn input coil of the flux transformer, while the direct-coupled loop was inductively coupled to the modulation/feedback coil of the SQUID electronics and also served as one of the superconducting electrodes for the current bias of the SQUID, as shown in Fig. 2. SQUIDs and flux transformers possessing the lowest intrinsic noise levels were selected for assembly of the flip-chip magnetometers.

The surfaces of the YBCO films were investigated using a JEOL 7400F SEM and an atomic force microscope (AFM) from Surface Imaging Systems. Lamellae for the investigation of samples using high-resolution transmission electron microscopy (HRTEM) were made using an FEI Helios Nanolab 400S focused ion beam (FIB) system. HRTEM images of step-edge junctions were taken using a Philips CM-20 microscope.

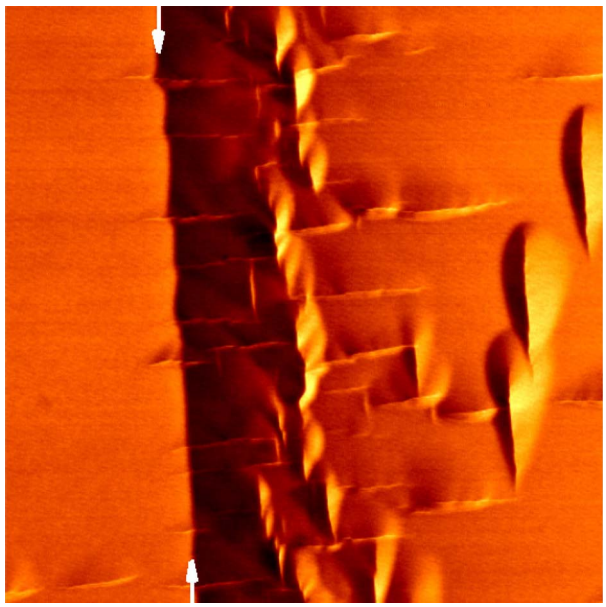

Fig. 3. AFM image acquired in PHASE mode of an ion beam textured surface of a step edge on a MgO substrate. The position of the upper corner of the step is marked by white arrows. The scan area is 5 μm $\times$ 5 μm.

The magnetometers were encapsulated in vacuum-tight sealed fiber-glass epoxy encapsulation together with a modulation coil and a Pt heater. AC-bias SQUID control electronics and a 1.5 liter LN_2 cryostat, both from Cryoton Ltd, were used for operation of the high-T_c magnetometer.

III. Results

The main results of this paper concern the study of step-edge junctions on MgO substrates as the active and most crucial parts of the magnetometer. After preparation of the 300 nm step by IBE, the AZ photoresist mask was removed using acetone and the MgO surface was etched additionally using an Ar ion beam along the [001] direction of the substrate for 30 min. This second etching of the MgO substrate with steps using IBE produced linear trenches along [100] and [010] directions on the surface, which are visible in PHASE images taken using an AFM in Fig. 3. These trenches were a few nm deep and served to align the a- and b-axes of the YBCO film normal to the corners of the step by graphoepitaxy: the preferred nucleation of YBCO near these trenches enhances the in-plane-oriented growth of the YBCO film on the MgO. The angle of the upper corner of the substrate step was about 40° relative to the substrate (001) plane. The effective width of the step edge is about 300 nm.

Fig. 4 shows an SEM image of an individual step-edge Josephson junction on an MgO substrate. The surface morphology of the grains in the YBCO film indicates that the orientation of the c-axis of the YBCO film on the step edge surface differs from the film orientation on the plane surface. SEM images of the step edge area made before lithography showed growth spirals with 1 nm steps on the surface of the grains, with the orientation of the a- or b-axes of the YBCO film aligned in-plane, normal to the corners of the step [17].

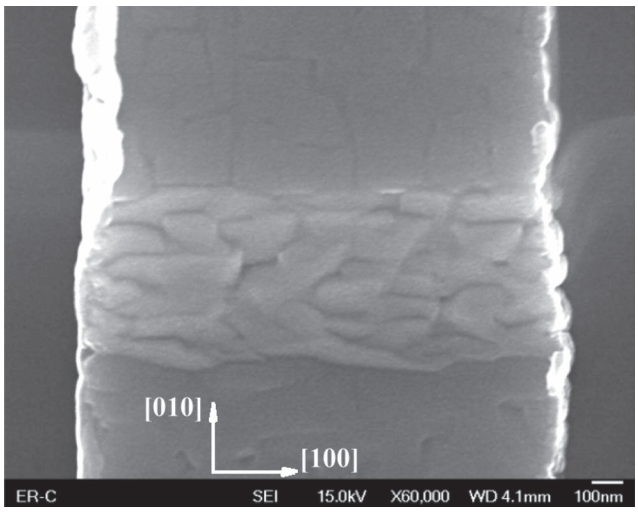

Fig. 4. SEM image of an individual step-edge Josephson junction on a MgO substrate. The orientation of the c-axis of the YBCO film on the step-edge surface differs from the film orientation on the plane surface.

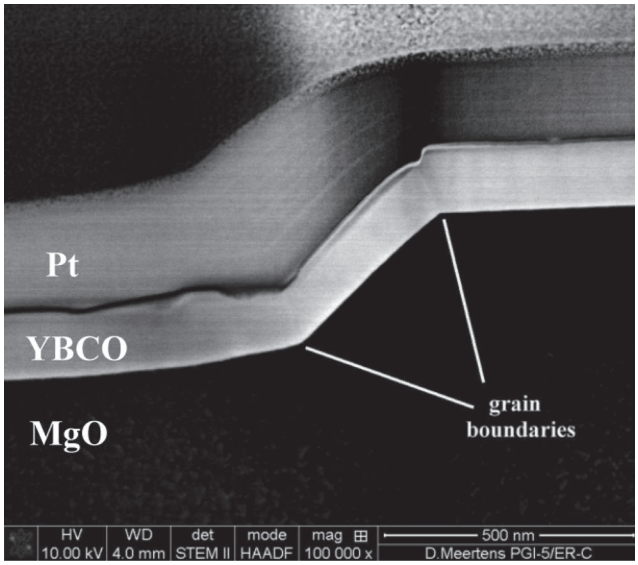

Fig. 5. High-angle annular dark-field TEM image of a step-edge Josephson junction on (001) MgO substrate. There are two grain boundaries: one on the top and one on the bottom of the step.

Two sharp changes in the YBCO film growth direction—one at the upper corner of the substrate step and the other at the lower corner of the substrate step—are clearly visible. These changes are associated with high-angle grain boundaries (GBs) in the YBCO film, in agreement with [18].

The two GBs can be distinguished in Fig. 5, which shows a high-angle annular dark-field TEM image of a step-edge Josephson junction on an (001) MgO substrate: one GB is on the upper corner and the other is on the lower corner of the step. The image was taken in a FEI Helios Nanolab 400 s FIB system after the preparation of a $\sim$100 nm thick lamella for HRTEM.

This lamella was transferred into a Philips CM-20 microscope and HRTEM images of both GB areas of the step-edge junction were taken. Fig. 6 shows an HRTEM image of the YBCO film deposited on the upper corner. The ab-planes of the film are not parallel to the surface of the edge, while the

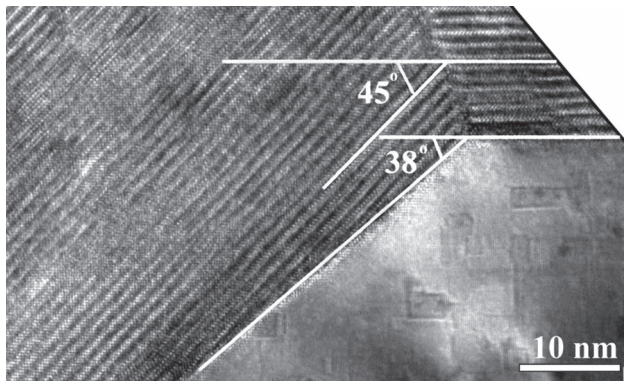

Fig. 6. HRTEM image of the YBCO film deposited on the upper corner of the substrate step.

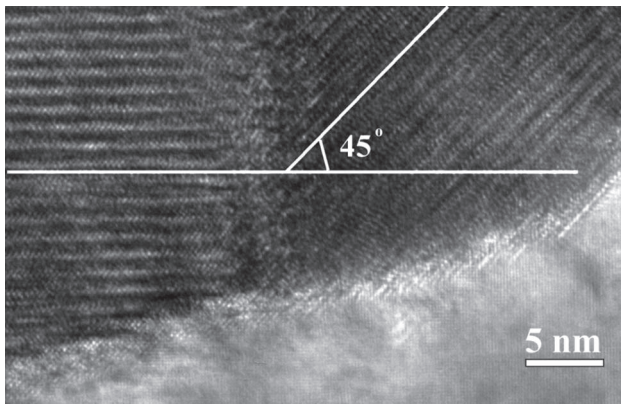

Fig. 7. HRTEM image of the YBCO film deposited on the lower corner of the substrate step.

GB has exactly a 45° misorientation. The c-axis of the YBCO film is oriented parallel to the [011] orientation of the MgO at the edge. This image shows a combination of graphoepitaxial in-plane and epitaxial out-of-plane growth of the YBCO film on the step edge of the MgO substrate. In contrast to [14], the c-axis of the YBCO film is not normal to the step edge surface but forms a near coincidence site lattice arrangement [19], [20], according to which the interfacial energy has primary minima at 0° (cube-on-cube) and 45° misorientations. This conclusion is confirmed in an HRTEM image of the YBCO film deposited on the lower corner of the substrate step (Fig. 7). The ab-planes of the YBCO film are oriented parallel to the (001) plane of the MgO up to a tilt of $\sim$20° of the MgO surface and parallel to the (101) plane of the MgO for a surface tilt angle exceeding 20° from the (001) plane of the MgO. A c-axis orientation of YBCO on a tilted MgO surface would require a significantly higher exposure during the second IBE process and/or the need to use an "antiepitaxial" buffer layer [21]. The c-axis oriented growth of YBCO on tilted or on (011) surfaces of MgO is also required for energy related applications such as making superconducting tapes using the inclined-substrate deposition (ISD) method [22].

The reproducibility of the step-edge Josephson junctions was sufficiently good, with a spread of critical currents of $\sim$20% and a value for I_cR_n of $\sim$300 μV at 77 K. Both the upper and the lower GBs of each step-edge junction have similar misorientation angles and cross-sections and, consequently, similar

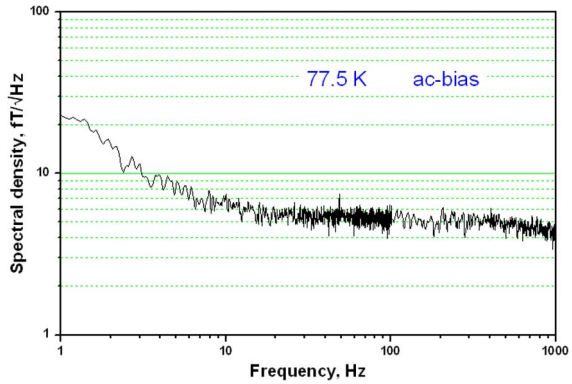

Fig. 8. Noise spectral density of the 16-mm high-T_c dc SQUID magnetometer with step-edge junctions measured in a superconducting shield.

critical currents and normal state resistances. They are serially connected and act together as a single Josephson junction with twice the normal state resistance R_n and half of the capacitance of a single GB. This is also beneficial for the high-frequency applications. The noise of the autonomous SQUIDs and SQUID magnetometers with step-edge junctions was similar to that obtained using 24° bicrystal Josephson junctions. Fig. 8 shows an example of the noise spectral density of the 16 mm high-T_c DC SQUID flip-chip magnetometer with step-edge junctions measured in a superconducting shield.

The properties of the 45° [100]-tilted GB of the step-edge junction are similar to those of the 22.5° [001]-tilted GB of a standard bicrystal Josephson junction, according to the angular dependence of the superconducting gap function for the d_{x2-y2} pairing symmetry in YBCO in momentum space:

$$\Delta(\vec{k}) \propto k_x^2 - k_y^2 = (\cos^2\varphi - \sin^2\varphi)\sin\theta = \cos(2\varphi)\sin\theta$$

where φ is the in-plane misorientation angle along the [001] axis and θ is the out-of-plane misorientation angle along the [100] axis.

The MEG measurements were performed in an MSR using both a one-channel high-T_c DC SQUID measurement system and a commercial 248-channel low-T_c MEG system (low-T_c SQUID magnetometers with 9 mm pickup coil; "Magnes 3600 WH" 4 D-Neuroimaging) [12]. The analog output from the high-T_c system was connected to a 16-bit analog-to-digital converter port available on the low-T_c system with a sampling rate of 678 Hz and processed together with the signals from the low-T_c magnetometers. The MSR provides a shielding factor $> 10^4$ for frequencies above 50 Hz. The residual magnetic flux density in the middle of the MSR is ~100 nT. The magnetic field resolution of the high-T_c system was ~5 fT/$\sqrt{\text{Hz}}$ with the high-T_c magnetometer operating at 77 K in the superconducting shield and ~7 fT/$\sqrt{\text{Hz}}$ (white noise level) at 77 K in the MSR. The low-T_c system had a magnetic field resolution of ~5 fT/$\sqrt{\text{Hz}}$ with the low-T_c SQUID operating at 4.2 K in the MSR.

Fig. 9 shows representative simultaneous measurements acquired with the low-T_c and high-T_c systems placed ~1 m from each other in the middle of the MSR. Both traces show real-time raw data obtained from the high-T_c and low-T_c magnetometers, low-pass filtered by the data acquisition system. Correlations

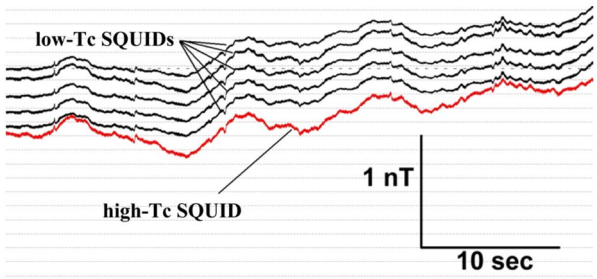

Fig. 9. Traces of signals obtained using high-T_c and low-T_c dc SQUID magnetometers.

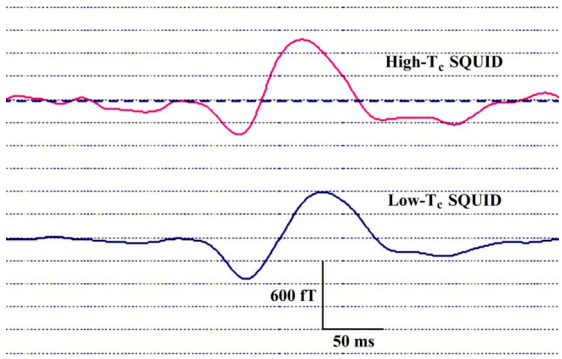

Fig. 10. Auditory evoked MEG signals acquired with the low-T_c whole-head system (lower curve) and the high-T_c system (upper curve).

between the traces result from ambient noise in the MSR and demonstrate the stability of operation of the high-T_c system.

Auditory signals were generated by electrostatic drivers outside the shielded room and the sound was transmitted via flexible tubes to the ears of the subject. Positions with maximum response obtained from whole-head recordings were used as starting positions for the high-T_c recordings. Measurements at 18 different positions around the maximum position were recorded. To establish a sensor coordinate system, the positions of the high-T_c sensor relative to the head frame were determined using the Fastrack system manufactured by Polhemus. Fig. 10 shows an example of auditory evoked MEG signals acquired with the low-T_c whole-head system and the high-T_c system. Both data sets show averages over 100 epochs and were band-pass filtered from 3 to 30 Hz. The traces obtained from both the high-T_c and the low-T_c systems demonstrate similar signal-to-noise ratios in spite of the 18 times difference in the operating temperatures of the sensors.

ACKNOWLEDGMENT

The authors thank the technical assistance of D. Meertens and R. Speen.

REFERENCES

[1] "Low helium supply, high prices affect balloons, MRIs," *CBC News*, Jun. 18, 2012. [Online]. Available: www.cbc.ca/news/canada/windsor/story/2012/06/18/wdr-helium-shortage.html
[2] C. Witchalls, "Nobel prizewinner: We are running out of helium," *New Scientist*, Aug. 18, 2010.
[3] C. Witchalls, "One minute with ... Robert Richardson," *The New Scientist*, vol. 207, p. 29, 2010.

[4] "Helium Privatization Act of 1996," in *Public Law 104-273, 104th Congr. (2nd Session)*, Oct. 9, 1996, [H.R. 4168].
[5] N. Kasai, K. Sasaki, S. Kiryu, and Y. Suzuki, "Thermal magnetic noise of dewars for biomagnetic measurements," *Cryogenics*, vol. 33, pp. 175–179, 1993.
[6] J. Nenonen, J. Montonen, and T. Katila, "Thermal noise in biomagnetic measurements," *Rev. Sci. Instrum.*, vol. 67, no. 6, pp. 2397–2405, 1996.
[7] Y. Zhang, Y. Tavrin, M. Mück, A. I. Braginski, C. Heiden, S. Hampson, C. Pantev, and T. Elbert, "Magnetoencephalography using high temperature rf SQUIDs," *Brain Topography*, vol. 5, no. 4, pp. 379–382, 1993.
[8] H. J. Barthelmess, M. Halverscheid, B. Schiefenhövel, E. Heim, M. Schilling, and R. Zimmermann, "Low-noise biomagnet ic measurements with a multichannel de-SQUID system at 77 K," *IEEE Trans. Appl. Supercond.*, vol. 11, pp. 657–661, 2001.
[9] F. Öisjöen, J. F. Schneiderman, G. A. Figueras, M. L. Chukharkin, A. Kalabukhov, A. Hedström, M. Elam, and D. Winkler, "High-Tc superconducting quantum interference device recordings of spontaneous brain activity: Towards high-Tc magnetoencephalography," *Appl. Phys. Lett.*, vol. 100, p. 132601, 2012, (4pp).
[10] M. I. Faley, C. L. Jia, L. Houben, D. Meertens, U. Poppe, and K. Urban, "Meandering of the grain boundary and d-wave effects in high-Tc bicrystal Josephson junctions," *Supercond. Sci. Technol.*, vol. 19, p. S195, 2006.
[11] 978-953-307-308-8M. I. Faley, "Epitaxial oxide heterostructures for ultimate high-Tc quantum interferometers," in *Appl. High-T_c Supercond.*, A. Luiz, Ed., 2011, pp. 147–176, InTech.
[12] M. I. Faley, U. Poppe, R. E. Dunin-Borkowski, M. Schiek, F. Boers, H. Chocholacs, J. Dammers, E. Eich, N. J. Shah, A. B. Ermakov, V. Y. Slobodchikov, Y. V. Maslennikov, and V. P. Koshelets, "Magnetoencephalography using a multilayer high-T_c DC SQUID magnetometer," *Phys. Proc.*, vol. 36, pp. 66–71, 2012.
[13] U. Poppe, N. Klein, U. Dähne, H. Soltner, C. L. Jia, B. Kabius, K. Urban, A. Lubig, K. Schmidt, S. Hensen, S. Orbach, G. Müller, and H. Piel, "Low-resistivity epitaxial $YBa_2Cu_3O_{7-x}$ thin films with improved microstructure and reduced microwave losses," *J. Appl. Phys.*, vol. 71, pp. 5572–5578, 1992.
[14] E. E. Mitchell and C. P. Foley, "YBCO step-edge junctions with high I_cR_n," *Supercond. Sci. Technol.*, vol. 23, p. 065007, 2010, (10pp).
[15] M. I. Faley, S. B. Mi, A. Petraru, C. L. Jia, U. Poppe, and K. Urban, "Multilayer buffer for high-temperature superconductor devices on MgO," *Appl. Phys. Lett.*, vol. 89, no. 8, p. 082507, 2006, (3pp).
[16] M. I. Faley, U. Poppe, K. Urban, D. N. Paulson, T. Starr, and R. L. Fagaly, "Low noise HTS dc-SQUID flip-chip magnetometers and gradiometers," *IEEE Trans. Appl. Supercond.*, vol. 11, no. 1, pp. 1383–1386, Mar. 2001.
[17] M. I. Faley, U. Poppe, D. Meertens, O. M. Faley, C. L. Jia, and R. E. Dunin-Borkowski, "Epitaxy and graphoepitaxy of oxide heterostructures on step edges," in *emc2012 Proceedings of the 15th European Microscopy Congress, 16th–21st September 2012, Manchester, UK*, vol. 1, *Physical Sciences: Applications*, D. J. Stokes and W. M. Rainforth, Eds., 2012, pp. 307–308, The Royal Microscopical Society, ISBN 978-0-9502463-5-2.
[18] C. P. Foley, S. Lam, B. Sankrithyan, Y. Wilson, J. C. Macfarlane, and L. Hao, "The effects of step angle on step edge Josephson junctions on MgO," *IEEE Trans. Appl. Supercond.*, vol. 7, pp. 3185–3188, 2001.
[19] D. M. Hwang, T. S. Ravi, R. Ramesh, S. W. Chan, C. Y. Chen, L. Nazar, X. D. Wu, A. Inam, and T. Venkatesan, "Application of a near coincidence site lattice theory to the orientations of $YBa_2Cu_3O_{7-x}$ grains on (001) MgO substrates," *Appl. Phys. Lett.*, vol. 57, pp. 1690–1692, 1990.
[20] R. W. Balluffi, A. Brokman, and A. H. King, *Acta Metall.*, vol. 30, pp. 1453–1470, 1982.
[21] M. I. Faley, "Reproduzierbarer Stufen-Josephson-Kontakt," Patent pending DE102012006825 (17.04.2012).
[22] M. Li, B. Ma, R. E. Koritala, B. L. Fisher, K. Venkataraman, V. A. Maroni, V. Vlasko-Vlasov, P. Berghuis, U. Welp, K. E. Gray, and U. Balachandran, "Pulsed laser deposition of c-axis untilted YBCO films on c-axis tilted ISD MgO-buffered metallic substrates," *Phys. C*, vol. 387, pp. 373–381, 2003.